

Manufacturing Letters

Manufacturing Letters 35 (2023) 991-998



51st SME North American Manufacturing Research Conference (NAMRC 51, 2023)

Detection and Identification of Particles on Silicon Wafers Based on Light Scattering and Absorption Spectroscopy and Machine Learning

Fengfeng Zhou^a, Xingyu Fu^a, Siying Chen^a, Martin B. G. Jun^{a,*}

^aSchool of Mechanical Engineering, Purdue University, 585 Purdue Mall, West Lafayette 47907-2088, USA

Abstract

Modern semiconductor manufacturing technology have a high-quality requirement of the wafers, and therefore the wafer inspection technique becomes increasingly important. During the manufacturing processes, particles can attach on the surface of the wafer which is an important factor of the quality and can even make it impossible to use the wafer. In this research, we introduce a particle detection and identification method based on the scattering and absorption spectra of the particles. A machine learning algorithm was developed to capture the feature of the particles and is able to identify the particle material from the scattering spectrum. Three different particles (Al₂O₃, SiC, and Si) were used to test this system. The validation accuracy achieves higher than 98% after 5 iterations training. The system was tested by scattering these three particles on the same wafer in different regions without mixing with each other. The results shows that particle Al₂O₃ and Si were identified with a high accuracy, whereas it is still challenging for the system to correctly label SiC particles. This can be improved by a larger dataset to enhance the generalization ability of the machine learning model.

© 2023 The Authors. Published by ELSEVIER Ltd. This is an open access article under the CC BY-NC-ND license (https://creativecommons.org/licenses/by-nc-nd/4.0)

Peer-review under responsibility of the Scientific Committee of the NAMRI/SME.

Keywords: wafer inspection, material identification, absorption spectrum, machine learning

1. Introduction

With the development of semiconductor industry, quality control of wafers becomes important. Early laser scattering methods used to detect the particles on the wafers are unable to identify the materials of the particles [1]–[3]. Visual inspection is still used to identify the materials of the particles and thus requires skilled technicians and is time consuming. Dou and Broderick [4] reported a new method to automatically detect particles and identify the materials, but the particle detection and material identification sub-systems are separated and therefore the whole system is complicated. Hattori and Koyata [5] developed a particle detection and identification system, but scanning electron microscopy (SEM) and energy dispersive X-ray spectroscopy (EDX) are used which is unaffordable to medium or small manufacturers. Therefore, cost-effective

automated system that is able to both detect and identify the particles is need.

In this research, we introduce a method to detect and identify the particles attached on the wafer surface using Light Scattering Spectroscopy (LiSSP) technology and machine learning algorithm. A beam of broadband light was used as the detection light to detect the particles. Since the detection light can be scattered to all the directions, it will be received by the optical fiber connected to the spectrometer. According to Mie scattering theory [6], scattered light is also a function of the refractive index of the material, the size of the particle, and the location of the observer. When the scattering angle and the particle size is fixed, the only factor that affects the scattering spectrum is the refractive index of the material. Since scattering is a process of light-matter interaction, absorption can also occur which further modifies the scattering spectrum.

^{*} Corresponding author. E-mail address: mbgjun@purdue.edu

Absorption spectrum is widely used in material monitoring and identification such as prediction of wafer quality, characterization of noble metal nanoparticles, etc. using UV-Vis absorption spectrum [7]–[9]. Therefore, it is possible to detect and identify the particles by the scattering spectrum. In order to capture sufficient hidden features in the scattered spectrum, a convolution neural network was developed to learn the labeled spectra obtained by the light scattered by different particles. 45870 spectra were collected to train the network and an accuracy of higher than 98% for the validation and testing set was obtained.

2. Method

2.1. Monitoring Principle

In this experiment, we tried to detect and identify the material of three different kinds of particles: SiC, Si, and Al₂O₃. From classic optics theory, the particles are excited by the time varying electric field of the detection light and introduce a time varying polarization. This time varying polarization then emits a new electromagnetic wave (light) to all the possible directions which is known as the scattered light. Therefore, when the particles are illuminated by the detection light, the light will be scattered everywhere. Moreover, due to the absorption of the particles, which is determined by the materials of the particles, the absorption of light with different wavelengths for different particles are different. In visible range, the different absorption can be directly observed by human eye as different colors. When the scattered light is received by a spectrometer, a different spectrum should be shown for different particles.

Since the size of the particles are much larger than the wavelength of the detection light (489.228 nm to 815.185 nm), large particle scattering occurs. As shown in Fig. 1, put the scatter on the origin of a spherical coordinate/Cartesian coordinate. The observer is on point A. The projection of OA on plane xOy is line section r_{xy} . Line section r_z is parallel with axis z. The plane expanded by r_{xy} and r_z is called the scattering plane. The scattering light can be given by the scattering matrix [6], [11]:

$$\begin{bmatrix} E_{\parallel s} \\ E_{\perp s} \end{bmatrix} = \frac{e^{ik(r-z)}}{-ikr} \begin{bmatrix} S_2(\theta) & 0 \\ 0 & S_1(\theta) \end{bmatrix} \begin{bmatrix} E_{\parallel i} \\ i \end{bmatrix}, \tag{1}$$

where S_j are elements of the amplitude scattering matrix, i is the imaginary unit. Here we only consider the elastic scattering, for which the wavelength of the scattered light is the same as the incident/detection light. The inelastic scattering, for which there is a shift of wavelength of the scattered light compared with the incident/detection light is weak compared with its elastic scattering counterpart. The elements of the scattering matrix of the far field are given by the multipole expansion [12]:

$$S_{1}(\Theta) = \sum_{n=1}^{\infty} \frac{2n+1}{n(n+1)} (a_{n}\pi_{n} + b_{n}\tau_{n})$$

$$S_{2}(\Theta) = \sum_{n=1}^{\infty} \frac{2n+1}{n(n+1)} (a_{n}\tau_{n} + b_{n}\pi_{n})$$
(2)

where

$$\pi_n = \frac{1}{\sin \theta} P_n^1(\cos \theta), \qquad \tau_n(\cos \theta) = \frac{d}{d\theta} P_n^1(\cos \theta), \quad (3)$$

 $P_n^1(\cos \theta)$ is the associated Legendre polynomial of the first kind, which is expected since we are solving the wave equation in spherical coordinates.

$$a_{n} = \frac{m\psi_{n}(m\alpha)\psi'_{n}(\alpha) - \psi_{n}(\alpha)\psi'_{n}(m\alpha)}{m\psi_{n}(m\alpha)\xi'_{n}(\alpha) - \xi_{n}(\alpha)\psi'_{n}(m\alpha)}$$

$$b_{n} = \frac{\psi_{n}(m\alpha)\psi'_{n}(\alpha) - m\psi_{n}(\alpha)\psi'_{n}(m\alpha)'}{\psi_{n}(m\alpha)\xi'_{n}(\alpha) - m\xi_{n}(\alpha)\psi'_{n}(m\alpha)}$$

$$(4)$$

where $\psi_n(x) = xj_n(x)$, $\xi_n(x) = xh_n^{(1)}(x)$ are the Riccati-Bessel functions. Here, the scattered light is independent of angle ϕ because of the cylindrical symmetry around z axis as shown in Fig. 1. $\alpha = 2\pi a/\lambda$ is the unitless size factor, where a is the radius of the sphere and λ is the wavelength of the incident/detection light in vacuum.

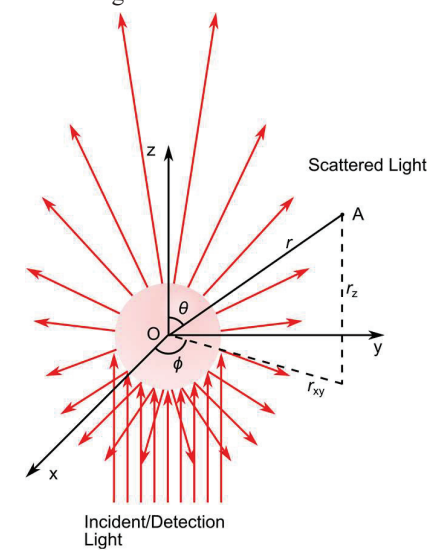


Fig. 1. Light scattered by a spherical particle with large diameter compared with the wavelength of the incident light.

Fig. 2 shows the scattered light of a SiC sphere (refractive index = 2.6353 at a wavelength of 632.8 nm incident light) with a diameter of 50 μ m. As we can see, the strongest scattering direction is 0° (the direction of the incident light). Then the intensity rapidly decreases as the scattering angle increases. Scattered light exists for all the directions, which agrees with the optical theorem which states that for plane incident light wave, the scattered light will propagate to all directions. This important phenomenon will be the key to eliminate the strong background light which will be introduced in section 2.2.

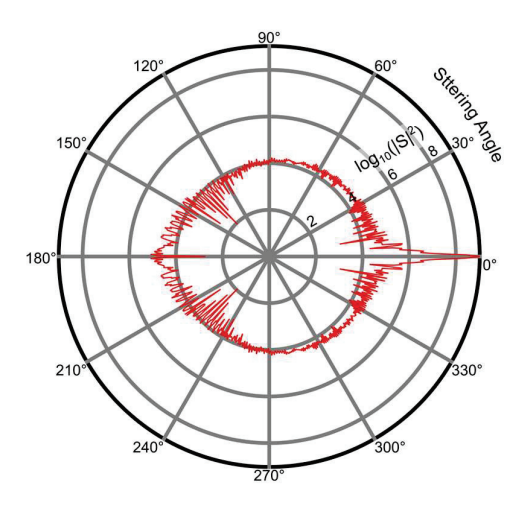


Fig. 2. Example of scattered light of a spherical SiC.

For elastic scattering, although the wavelength of the scattered light will not be changed, the scattering intensity for a specific wavelength of incident/detection light can be different for different materials. This phenomenon is due to the interaction between light and the atomic/molecular structure of the scatter. Fig. 3 shows a schematic drawing of the principle of the scattering spectroscopy. Assume a broadband light is used as the incident light as shown in Fig. 3 (b), after scattered, due to the different scattering intensity for different wavelengths, the light with a wavelength colored as yellow has a lower scattering intensity and the scattered spectrum is distorted as shown in Fig. 3 (c). Therefore, if a broadband light is used as the incident/detection light, the spectrum of the scattered light is determined only by the material of the scatter. For different materials, the scattered light can be different. Therefore, Light Scattering Spectroscopy (LiSSP) technology is used to identify the material of the scatter. By constructing a one-to-one mapping between the material of the scatter and the scattering spectrum, the material of the scatter can be determined by observing the characteristics of the scattering spectrum. Therefore, the key to identify the materials of the particles is that the scattering spectrum of the materials are different.

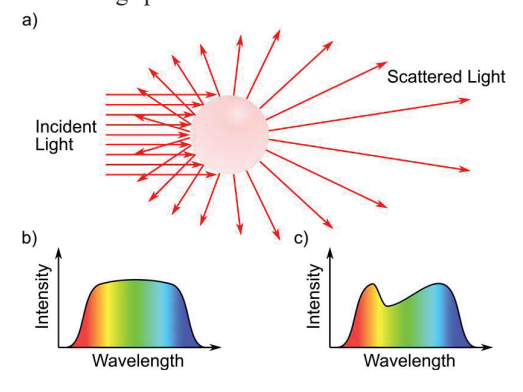


Fig. 3. Schematical illustration of light scattering spectroscopy. a) the light scattering process; b) the spectrum of the incident/detection light; c) the spectrum of the scattered light.

2.2. System Setup

The particle identification system consists of the 4 parts: the motion part, the illumination part, the receiving part, and the analyzing part. The motion part is the subsystem that move the wafer so that it can be scanned by the detection system. The illumination part includes the light source and the light delivering optical fiber (Lead-In Fiber). The receiving part includes the light receiving fiber (Lead-Out Fiber) and the spectrometer. The analyzing part is the analyzing algorithm that is able to detect particles and identify the materials. Fig. 4 shows the drawing of the wafer inspection system. A broadband light source (Thorlabs, MBB1F1, wavelength 470 nm to 850 nm) in the visible range was used to provide the detection light. The light was guided by the Lead-In Fiber to illuminate the particles on the wafer. Then, the scattered light will be received by the Lead-Out fiber to the spectrometer (Ocean Optics, USB2000+, wavelength 489.228 nm to 815.185 nm). A 6-axis Hexapod (ALIO, Hybrid Hexapod, positioning precision < 100 nm) was used to spin and move the wafer so that the surface of the wafer can be scanned by the detection light.

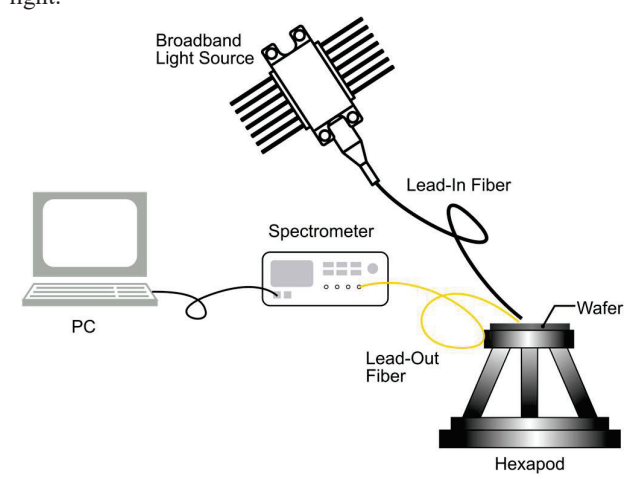


Fig. 4. Drawing of the wafer inspection system.

Polymer optical fiber (MIKROE - 1473, NA = 0.5) with a core diameter of 980 µm was used as the Lead-In Fiber. However, when the light exits the fiber, a significant divergence will occur which will reduce the power density of the illumination light. For small particles, a high-power density of the illumination light is required so that the scattered light is strong enough to have a high signal to noise ratio (SNA). To increase the power density, a convex lens was made on the exit side of the optical fiber to focus the light so that the power density can be improved. Fig. 5 a) and b) shows the image of two polymer optical fibers (POFs) without and with convex lens, respectively. The lens was made using clear UV curable resin. A drop of resin was attached to tip of the POF. Due to the surface tension, the resin shrinks and forms a spherical shape with a smooth surface. Then, the light exit from the fiber will be focused and the power density of the detection light will be increased.

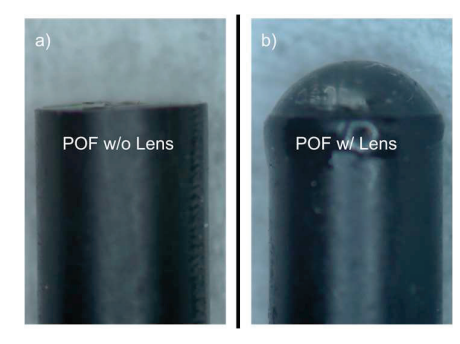


Fig. 5. Microscope image of polymer optical fiber (POF) with and without lens. a) POF without lens on the fiber; b) POF with lens on the fiber.

Fig. 6 shows the measurement of the intensity distribution of the light exit from the POF with lens. Fig. 6 a) shows the method to measure the light intensity distribution. A beam profiler (Thorlabs, BC106-VIS) was used to measure the 2-D intensity distribution of light projected on the sensing surface. A single mode optical fiber (SMF) was attached with the POF firmly to conduce non-contact measurement of the initial distance between the SMF and the Beam Profiler (L_0) using the method introduced in Ref. [13]. The distance between the tip of the SMF and the POF (L_1) was also measured using a microscope. The measurement of L_0 and L_1 are conducted only once before the measurement of the beam profile of the light. The initial distance between the POF and the Beam Profiler is $L = 676 \,\mu\text{m}$. After measurement of the initial distance and the beam profile, the POF was moved away from the Beam Profiler and the movement was measured using a linear encoder. The beam profile was then measured for every movement of 0.1 mm. Fig. 6 b) shows the intensity distribution of the light exit the POF. The distance between the POF and the Beam Profiler increase along z axis. As we can see, we have a minimum light spot size when the Beam Profiler is close to the POF. The size increases with the increase of the distance between the Beam Profiler and the POF. This is because the divergence of the light of the POF without the lens is high, and the lens only helps to reduce the divergence but was not able to focus the light into a small spot. The beam size along y direction at L = 0.676 mm is 1.12 mm, and at L = 5.676 mm is 3.13 mm (with respect to 1/e of the maximum intensity). By reducing the divergence of the detection light, the power density of the detection light can be improved.

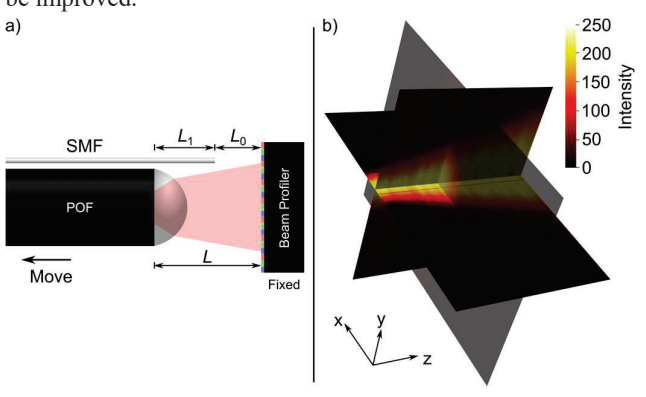


Fig. 6. Measurement of the intensity distribution of the light exit the POF with lens. a) the measurement method; b) the intensity distribution, width (x direction) 8.78 mm, height (y direction) 6.6 mm, length (z direction) 5 mm.

Fig. 7 shows the detection of scattered light and the relationship between the fibers and the wafer. In Fig. 7 a), a beam of Detection Light come from the Lead-In Fiber and is reflected by the wafer. The incident angle of the Detection Light is 45°. Therefore, when there is no particle on the wafer, all the light is reflected by the mirror surface of the wafer with a reflection angle of 45°. The Lead-Out Fiber is on the same side of the Detection Light and therefore no reflection light can be received by the Lead-Out Fiber. Fig. 7 b) shows when the Detection Light hits the particle, the light is scattered to every and therefore can be detected by the Lead-Out Fiber. In this experiment, two POFs (Thorlabs, BFY200LS02, wavelength 400 nm to 2200 nm, NA = 0.39) were used to collect the scattered light and then coupled into one POF and sent into the spectrometer to improve the sensitivity. Fig. 7 c) shows the front view of the Lead-In Fiber and the Lead-Out Fibers. The angle between the Lead-In Fiber and the Lead-Out Fibers are 30°, all the three fibers points to the same position so that the particle on the wafer can be detected. Fig. 7 d) shows the side view of the three fibers. As we can see, in the side view the three fibers overlap and therefore we can only see one fiber. All the three fibers have a 45° angle with the surface of the wafer. Therefore, when the spectrometer receives a strong light, it means a particle is detected.

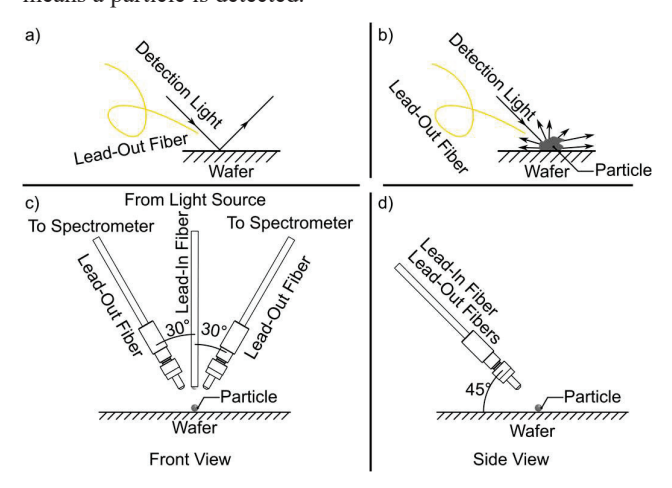


Fig. 7. Lead-In and Lead-Out fiber to lunch detection light and detect scattered light. a) and b) principles of scattered light detection; c) and d) front view and side view of the Lead-In and the Lead-Out fibers.

2.3. Spectrum Analysis

There are two goals in this experiment: first we need to detect the particles on the wafer, and second we need to identify the material of the detected particles. To detect the particles, we only need to focus on the intensity of the light received by the spectrometer. Fig. 8 shows the spectra when no particle was detected by the system and a particle was detected by the system. As we can see, when there was no particle, the spectrum has a low intensity. This is because most of the detection light is reflected by the mirror surface of the wafer, and the light received by the spectrometer is due to the impurity of the material of the lens which also cause a weak scattering. When a particle is detected by the system, the intensity of the spectrum increases dramatically and can be easily distinguished from that when there is no particle. The easiest

way to compare these two spectra is taking the summation of the intensity of all the sampling points:

$$I = \sum I_{\lambda},\tag{5}$$

where I_{λ} is the intensity of a specific sampling point with wavelength λ . With this method, a spectrum with multiple sampling points becomes a single number which is easier to compare and requires less memory space.

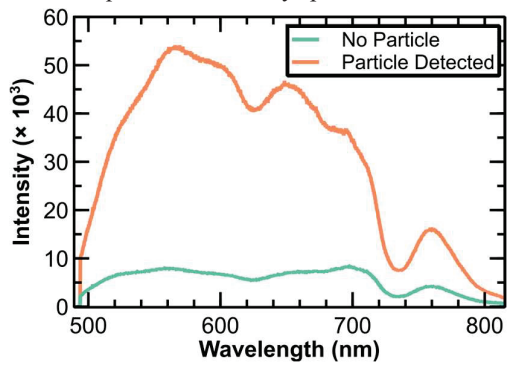


Fig. 8. Spectra when no particle is detected (green) and a particle is detected (orange).

To detect the particles on the wafer, all the surfaces of the wafer should be scanned. The strategy to scan the wafer is spin the wafer for one full cycle with a distance between the center of the wafer and the detection point of r, and then shift the wafer for a distance d and repeat the scan process until all the position of the wafer is scanned. It should be noted that since we want the particle spends the same amount of time under the detection light when detected, we need to keep the line speed constant instead of the angular speed. Therefore, the angular spin speed should be

$$\omega(r) = v/r,\tag{6}$$

where v is a constant and r is the distance between the scanned point and the center of the wafer. Fig. 9 shows the scan result of one Al₂O₃ particle on the surface of the wafer with a scan speed of v = 0.5 mm/s and a sampling frequency of 10 Hz. In this plot, each point is the value calculated from Eq. (5). As we can see, a slow varying periodical pattern is observed which is because of the pitch of the wafer. When the wafer spins, some places are closer to the fibers which is shown as a relatively higher intensity. With this periodical pattern we can determine how many cycles the wafer spins and the relative position of the particles detected by the system. Also, three peaks labeled as Al₂O₂ are detected. These are due to the Al₂O₃ particle we want to detect. Since these three peaks are located in the same position according to the periodical pattern and we have only one Al₂O₃ particle, these are caused by the same particle because the spot size of the detection light is slightly larger than the shift d of two adjacent scanning cycles. The other weaker peaks are caused by the dusts attached on the wafer during the scanning process.

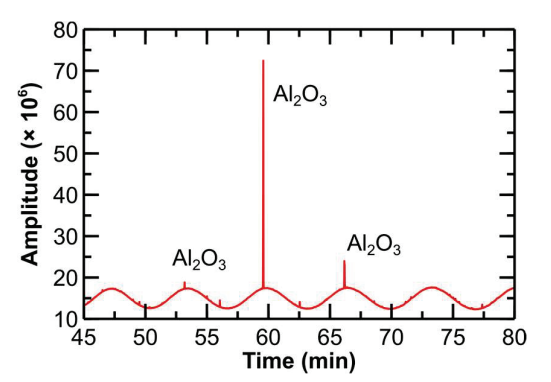


Fig. 9. Scan result of one Al_2O_3 particle on the surface of the wafer with a constant scan speed of $\nu=0.5$ mm/s.

For the second goal, identification of the particle materials, we need to compare the scattering spectrum of each material. Fig. 10 shows the scattering spectra received by the spectrometer of different particle materials. Differences between these spectra can be seen especially in the shaded region. This is because of the different extinction coefficients for a specific wavelength of the detection light cause by the atomic and molecular structure of the material. However, it is difficult for humans to learn and identify all the characteristics of the spectra since it is also possible that the spectra may be distorted by some known or unknown reasons. Fortunately, machine learning algorithms do a good job of extracting the hidden characteristics of data. In this experiment, a convolution neural network (CNN) will be used to learn the characters of the spectra of the materials. Scattering spectra under different measurement conditions produced by known materials will be used to train the CNN model. After training, a wafer with mixed particles on the surface will be used to test the performance of the model.

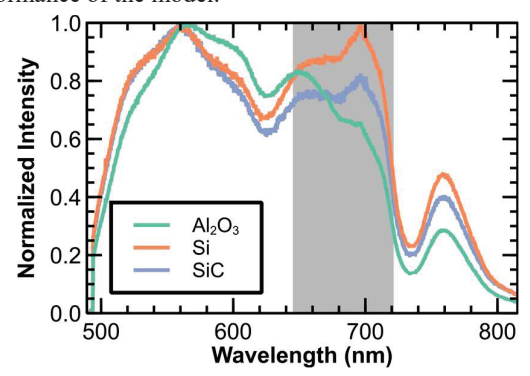


Fig. 10. Scattering spectra of different particles.

3. Result and Discussion

Three different kinds of particles ($44\sim149~\mu m$): Al₂O₃, SiC, and Si were used in the experiment. The particles were scattered randomly on the wafer. The distance between the optical fibers and the surface of the wafer was set as 3 mm. The scan speed and the shift speed were set as 0.5 mm/s and kept as constant during the scan process. Then the wafer spins with an angular speed is a function of the distance of the scan point and the center of the wafer calculated by Eq. (6). The sampling rate of the spectrometer was set as 10 Hz. Fig. 11 shows the

measurement result of the system. As we can see, the slow varying periodical pattern is due to the pitch of the wafer. It should be noted that the period reduces with time. This is because the system scans the wafer from its edge to the center. Since the line speed is a constant, the angular speed increases with the reduction of the radius r. Large number of peaks can be seen, which is because of the particles detected by the system.

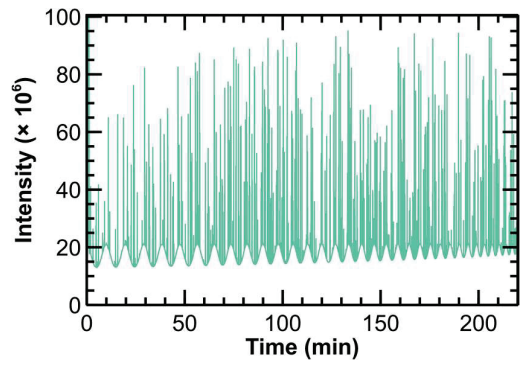


Fig. 11. Detection of particles on the surface of the wafer.

Since we know the scan speed and the time of the sampled point, it is possible to reconstruct the distribution of the particles. Fig. 12 shows the particle distribution on the wafer. A bright strip on the edge of the of the wafer can be seen, which was caused by the primary flat that the holder under the wafer was illuminated by the detection light and large amount of light was scattered everywhere. With the reconstructed surface, we can easily find the distribution of the particles and evaluate the quality of the wafer.

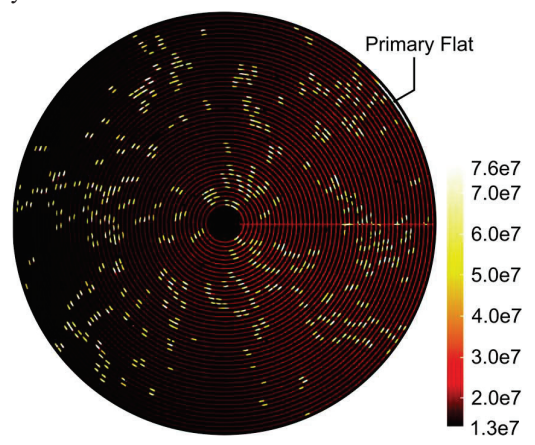
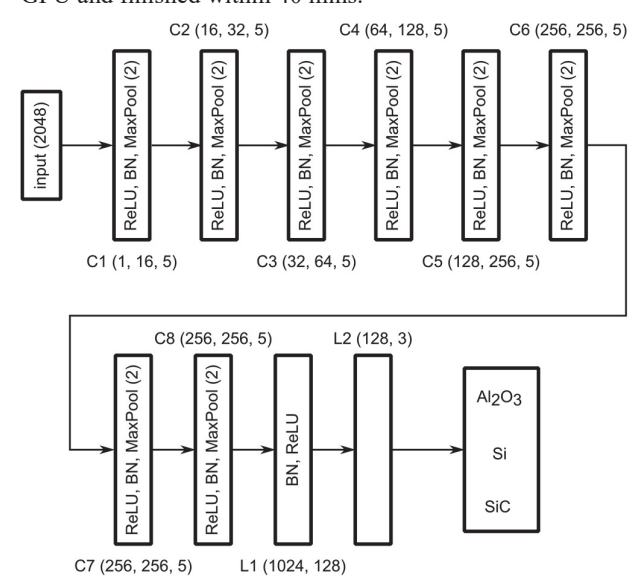


Fig. 12. Reconstruction of the particle distribution on the surface of the wafer.

A supervised learning model was developed to learn the features of the spectra of particles with different materials. Fig. 13 shows the architecture of the model. Each input spectrum has 2048 sampling points. 8 convolution layers were used to capture the features from different levels. We follow vanilla CNN structure as the backbone and use grid search to fine tune our model which is shown in Fig. 13. Cross entropy loss was used as the loss function, Adam (learning rate = 10^{-5}) was used as the optimizer. 45870 normalized and labeled spectra (Al₂O₃ = 21189, Si = 14560, SiC = 10121) were used to train the model. Al₂O₃, Si, and SiC were labeled as 0, 1, and 2,

respectively. The dataset was separated by 0.7, 0.15, 0.15 as training, validation, and testing datasets, respectively. The batch size was set as 128. Since we are using an imbalanced dataset, the weight for calculating the cross-entropy loss was set as 0.2196, 0.3204, and 0.4600 for Al₂O₃, Si, and SiC, respectively. The training was conducted on a personal computer with a Intel I7 8700K CPU and a Nvidia RTX 3090 GPU and finished within 40 mins.



*Note: C (a, b, c) denotes convolution layer (input channel, output channel, kernal size); L (a, b) Linear Layer (input feature, output feature); BN BatchNorm1d; MaxPool1d (kernel size).

Fig. 13. Architecture of the CNN model to identify the materials of the particles from their scattering and absorption spectra.

Fig. 15 shows the training and testing history of the mode. As we can see, training accuracy increase quickly after several iterations. Testing accuracy and validation accuracies are slightly lower than the training accuracy. After 5 iterations all the accuracies reaches 98%. Fig. 15 b) shows the training, testing, and validation losses. As we can see, the loss reduces quickly below 0.5×10^{-3} after 10 iterations. After 20 iterations, the loss becomes stable and start to oscillate around 0.25×10^{-3} . The confusion matrix is

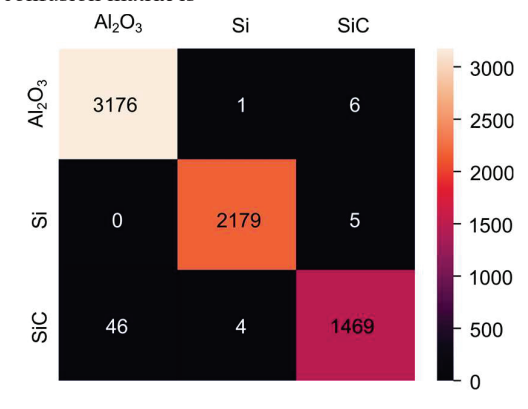


Fig. 14 | Confusion matrix of the training result.

The confusion matrix shows that most spectra can be labeled correctly. SiC can be labeled as Al_2O_3 by mistake, whereas there is a lower chance to incorrectly label Al_2O_3 as SiC.

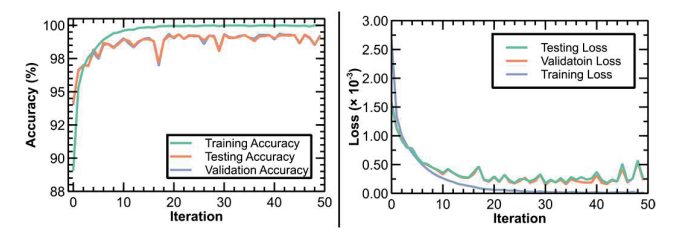


Fig. 15. Training and Testing history of the CNN model to identify the materials of the particles based on the scattering spectrum.

To test the CNN model in a real application, the surface of a wafer was divided into three equal sections (Region 1, Region 2, Region 3), each region has a central angle of 120°. Al₂O₃, Si, and SiC particles were scattered on Region 1, Region 2, and Region 3, respectively. No different particles were mixed in the same region. Fig. 16 shows the result of the CNN model, the black, red, and yellow color represents Al₂O₃, Si, and SiC particles, respectively. The distribution of particles in regions is given by Table 1. By considering Al₂O₃ and Si, but assuming SiC, the prediction accuracy is given by

$$a = \frac{CP_{\text{Al}_2O_3} + CP_{\text{Si}}}{T},\tag{7}$$

where $CP_{\mathrm{Al_2O_3}}$ is the correct prediction of $\mathrm{Al_2O_3}$, CP_{Si} is the correct prediction of Si, T is the total number of particles. Therefore, the prediction accuracy for particle Al₂O₃ and Si, the classification accuracy is 85.7% according to Table 1. However, the classification accuracy of SiC is low since large amount of SiC particles were labeled as Al₂O₃. For Region 1 (Al₂O₃) and Region 2 (Si), the particle predicted by the CNN model agrees well with the real particles scattered on that region. However, in Region 3, it is difficult for the CNN model to identify Al₂O₃ and SiC particles. This may because of the generalization ability of the CNN model is still limited to identify the difference of the spectra of these two particles. The environment noise (such as wafer's profile/waviness error, noise from the spectrometer, particle properties), other than the spectrum of the particles, might be learned by the model and therefore cause confusion between Al₂O₃ and SiC although in the testing set these two particles can be identified. This can be improved by creating a larger dataset, with different size of the particles on different wafers to mitigate the influence of the environment noise. Also, from Table 1 we know this model tends to incorrectly predict SiC as Al₂O₃ but unlikely to predict Al₂O₃ as SiC. This agrees with the confusion matrix Eq. (7). However, the probability to incorrectly label SiC as Al₂O₃ is much larger than that given by the confusion matrix.

Table 1. Distribution of particles in different regions, number in parentheses is the percentage of the particle in the region.

	•	-	
	Al_2O_3	Si	SiC
Region 1	5693 (81.4%)	1252 (17.9%)	53 (0.8%)
Region 2	847 (10.9%)	6934 (88.8%)	24 (0.3%)
Region 3	8980 (63.9%)	1475 (10.5%)	3595 (25.6%)

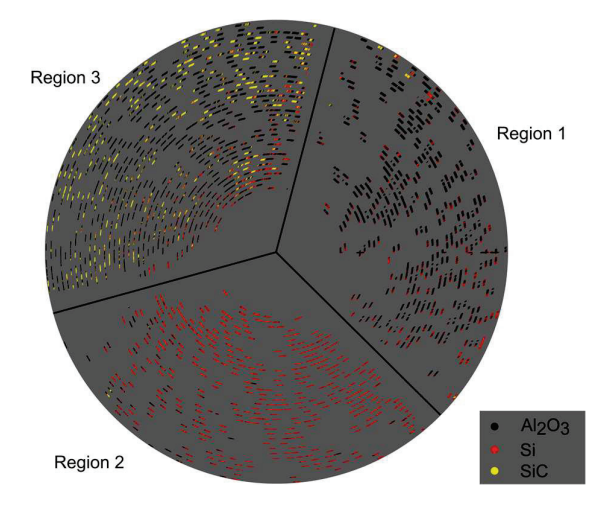


Fig. 16 | Material identification using the CNN model.

4. Conclusion

In this research, we developed an optical inspection system to detect and identify Al₂O₃, Si, and SiC particles attached on the wafer based on the scattering and absorption spectrum. The system consists of a 6-axis hexapod, a broadband light source, a Lead-In Fiber with a convex lens, two Lead-Out Fibers, a spectrometer, and a CNN model. The detection light was focused by the convex lens on the Lead-In Fiber the enhance the power density, and the scattered light was received by the two Lead-Out Fibers. The Hexapod spins and moves the wafer so that all the surface of the wafer can be scanned by the detection light. The scattered spectrum was recorded by the spectrometer and analyzed by the particle model and the CNN model. The particle detection model was used to detect the location of the particles so that the spectra of the particles can be correctly selected to train the CNN model. The training result shows that the model has a validation accuracy and a testing accuracy higher than 98% after 5 iterations training. The model was used to predict the material of the particles on a wafer, where the particles were located in different regions without mixing with each other. The testing result shows that the CNN model was able to identify the materials with a high accuracy for Al₂O₃ and Si but has a high risk to mislabel SiC as Al₂O₃. This may because of the insufficient ability of generalization of the model. To solve this problem, a larger training dataset is needed. Compared with other wafer inspection systems, this system can detect, locate, and identify the material of the particles simultaneously. Also, this system is cost-effective since other systems which are able to identify the material of the particles use expensive equipment such as SEM and EDX.

Acknowledgements

This material is based upon work supported by the National Science Foundation under Grant No. NSF AM-2125826.

References

- [1] K. Takami, "Defect inspection of wafers by laser scattering," *Materials Science and Engineering: B*, vol. 44, no. 1, pp. 181–187, Feb. 1997, doi: 10.1016/S0921-5107(96)01745-X.
- [2] S. Takahashi, T. Miyoshi, Y. Takaya, and K. Saito, "In-Process Measurement Method for Detection and Discrimination of Silicon Wafer Surface Defects by Laser Scattered Defect Pattern," *CIRP Annals*, vol. 47, no. 1, pp. 459–462, Jan. 1998, doi: 10.1016/S0007-8506(07)62874-1.
- [3] M. S. Kim, H.-S. Choi, S. H. Lee, and C. Kim, "A high-speed particle-detection in a large area using line-laser light scattering," *Current Applied Physics*, vol. 15, no. 8, pp. 930–937, Aug. 2015, doi: 10.1016/j.cap.2015.04.042.
- [4] L. Dou and M.-P. Broderick, "A new technique for automated wafer inspection and classification of particles and crystalline defects," in 1997 IEEE/SEMI Advanced Semiconductor Manufacturing Conference and Workshop ASMC 97 Proceedings, Sep. 1997, pp. 180–184. doi: 10.1109/ASMC.1997.630730.
- [5] T. Hattori and S. Koyata, "Applications of an automated particle detection and identification system in VLSI wafer processing," in *Integrated Circuit Metrology, Inspection, and Process Control V*, 1991, vol. 1464, pp. 367–376

- [6] G. Mie, "Contributions to the optics of turbid media, particularly of colloidal metal solutions," *Contributions to the optics of turbid media*, vol. 25, no. 3, pp. 377–445, 1976.
- [7] Y. Dai, H. Wang, J. Wang, X. Wang, Z. Wang, and X. Ge, "Prediction of water quality based on SVR by fluorescence excitation-emission matrix and UV–Vis absorption spectrum," *Spectrochimica Acta Part A: Molecular and Biomolecular Spectroscopy*, vol. 273, p. 121059, 2022.
- [8] R. Begum *et al.*, "Applications of UV/Vis spectroscopy in characterization and catalytic activity of noble metal nanoparticles fabricated in responsive polymer microgels: a review," *Critical reviews in analytical chemistry*, vol. 48, no. 6, pp. 503–516, 2018.
- [9] H.-H. Perkampus, *UV-VIS Spectroscopy and its Applications*. Springer Science & Business Media, 2013.
- [10] C. F. Bohren and D. R. Huffman, *Absorption and scattering of light by small particles*. John Wiley & Sons, 2008.
- [11] J. E. Hansen and L. D. Travis, "Light scattering in planetary atmospheres," *Space science reviews*, vol. 16, no. 4, pp. 527–610, 1974.
- [12] F. Zhou, W. Duan, X. Li, J.-T. Tsai, and M. B. G. Jun, "High precision in-situ monitoring of electrochemical machining process using an optical fiber Fabry–Pérot interferometer sensor," *Journal of Manufacturing Processes*, vol. 68, pp. 180–188, Aug. 2021, doi: 10.1016/j.jmapro.2021.07.010.